Optochemical Biology | Hot Paper

DOI: 10.1002/anie.201405355

Sequential Gene Silencing Using Wavelength-Selective Caged Morpholino Oligonucleotides**

Sayumi Yamazoe, Qingyang Liu, Lindsey E. McQuade, Alexander Deiters, and James K. Chen**

Abstract: *Spectrally differentiated caged morpholino oligonucleotides (cMOs) and wavelength-selective illumination have been used to sequentially inactivate organismal gene function. The efficacy of these reverse-genetic chemical probes has been demonstrated in zebrafish embryos, and these reagents have been employed to examine the mechanisms of mesoderm patterning.*

Photoactivatable molecules are versatile probes of cellular and organismal physiology, as they allow biochemical control with spatiotemporal precision.[1] We and others have developed caged morpholino oligonucleotides (cMOs) that can perturb targeted RNAs in vivo,[2–8] and these optochemical tools have been used to interrogate the functions of individual genes, such as the zebrafish transcription factors *no tail a* (*ntla*) and *ets variant gene 2* (*etv2*).[9,10] Morpholino (MO) systems that can similarly decipher the combinatorial actions of two or more genes would extend this approach to more complex biological systems; however, current cMOs have overlapping spectral properties that preclude differential control. Here we report the development of spectrally differentiated cMOs that enable sequential gene silencing through wavelength-selective illumination. We demonstrate the efficacy of these probes in zebrafish embryos and use them to examine the mechanisms of mesoderm patterning.

Our approach builds upon our previous studies of cyclic cMOs in zebrafish models.[7] Antisense MOs are typically 25 bases in length and designed to complement splicing or translational start sites in targeted RNAs. The resulting MO/RNA duplexes have limited tolerance for backbone curvature, and the MO activity can therefore be caged by cyclizing the oligonucleotide with a photocleavable linker. Illumination then relinearizes the antisense reagent and restores its function. MO cyclization has certain advantages over earlier caging methods, which utilize hairpin structures,[2,3] MO/RNA or MO/MO duplexes,[4,6] or modified bases:[5] cyclic cMOs are easy to synthesize, rely on a single optically gated trigger, and obviate the need for auxiliary oligonucleotides.

As a consequence of their modular design, cyclic cMOs can be prepared with a variety of linkers, and our first-generation reagents utilized tethers based on 4,5-dimethoxy-2-nitrobenzyl (DMNB), which are readily cleaved by light at a wavelength of 365 nm. The experimental scope of these reagents would be significantly expanded if cMOs targeting distinct RNA sequences could be differentially photoactivated. Wavelength-selective photo-deprotection of thiols has been achieved using 2-nitrobenzyl (NB) and ([7-bis(carboxymethyl)amino]coumarin-4-yl)methyl (BCMACM) chromophores,[11] and cyclic guanosine monophosphate (cGMP) and cyclic adenosine monophosphate (cAMP) signaling has been separately regulated using NB-caged protein kinase G and BCMACM-caged cAMP, respectively.[12] In addition, 4-carboxymethoxy-5,7-dinitroindolinyl-caged glutamate and BCMACM-caged γ-aminobutyric acid have been used to achieve bimodal control of each neurotransmitter,[13] and phosphoamino acids have been selectively caged with 1-(2-nitrophenyl)ethyl and [7-(diethylamino)coumarin-4-yl]-methyl (DEACM) groups.[14] We therefore envisioned that NB- and DEACM-based linkers could be used to develop wavelength-selective cMOs, thus allowing the sequential inactivation of two genes in whole organisms (Figure 1).

We first prepared a NB-containing linker with *N*-hydroxysuccinimide ester and chloroacetamide groups, which can react with 5′-amine- and 3′-disulfide-functionalized MOs to generate macrocyclic oligonucleotides. In comparison to our previous DMNB-based tether, this photocleavable linker has a blue-shifted absorption maximum, which minimizes photolysis at wavelengths greater than 400 nm. The bifunctional reagent was synthesized from commercially available 1-(2-nitrophenyl)ethane-1,2-diol (**1**) in eight steps (Scheme 1). The primary alcohol of **1** was tosylated and treated with methylamine, and the resulting 1,2-amino alcohol **2** was condensed with methyladipoyl chloride to yield the ester **3**. The secondary alcohol in **3** was then conjugated with ethylenediamine through 1,1-carbonyldiimidazole (CDI) mediated activation, and the primary amine was capped with 2-chloroacetyl chloride to yield compound **4**. Subsequent hydrolysis of the methyl ester and coupling with *N*-hydroxysuccinimide provided the fully functionalized NB linker **5**.

[*] Dr. S. Yamazoe,[+] Dr. L. E. McQuade, Prof. Dr. J. K. Chen
Departments of Chemical and Systems Biology and Developmental Biology, Stanford University School of Medicine
269 Campus Drive, CCSR 3155, Stanford, CA 94305 (USA)
E-mail: jameschen@stanford.edu
Homepage: http://chen.stanford.edu

Q. Liu,[+] Prof. Dr. A. Deiters
Department of Chemistry, University of Pittsburgh
Chevron Science Center
219 Parkman Avenue, Pittsburgh, PA 15260 (USA)
E-mail: deiters@pitt.edu
Homepage: http://www.pitt.edu/~deiters

[+] These authors contributed equally to this work.

[**] This work was supported by the NIH (R01 GM087292 and DP1 HD075622 to J.K.C.; R01 GM079114 to A.D.), a Japan Society for the Promotion of Science Fellowship (to S.Y.), and an A. P. Giannini Foundation Fellowship for Medical Research (to L.E.M.)

Supporting information for this article is available on the WWW under http://dx.doi.org/10.1002/anie.201405355.

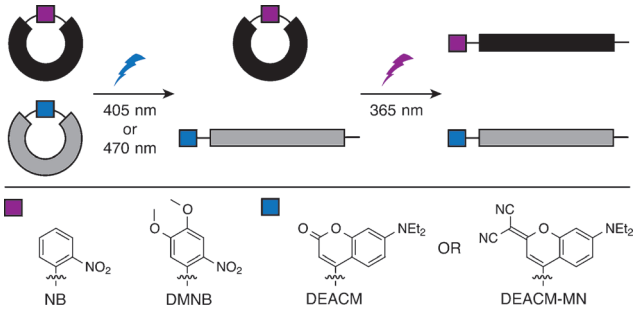

Figure 1. Sequential activation of cyclic cMOs using different wavelengths of light. Structures of spectrally differentiated caging groups are shown.

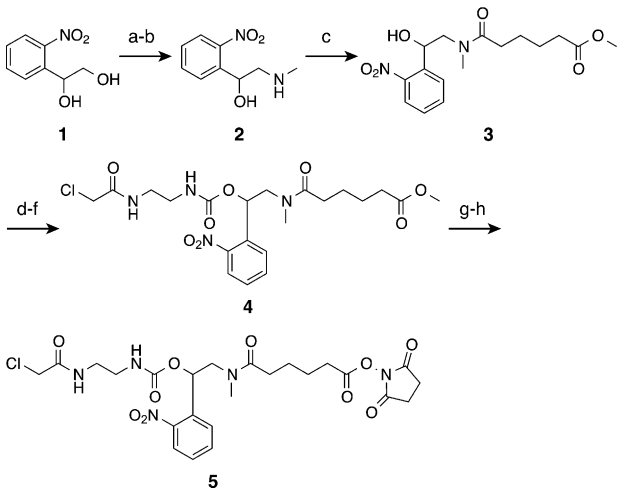

Scheme 1. NB linker synthesis. a) TsCl, pyridine, 99%; b) methylamine, THF, 91%; c) methyladipoyl chloride, DIPEA, CH_2Cl_2, 41%; d) CDI, CH_2Cl_2; e) ethylenediamine, CH_2Cl_2; f) 2-chloroacetyl chloride, Et_3N, CH_2Cl_2, 65% over 3 steps; g) LiOH, THF, H_2O; h) DSC, pyridine, CH_3CN, 62% over 2 steps. Ts = toluene-sulfonyl, DIPEA = *N*,*N*-diisopropylethylamine.

We next prepared two DEACM-based linkers with differing absorption properties. The addition of electron-donating groups to the C7-position of the coumarin ring induces a bathochromic shift, and DEACM protecting groups are efficiently photolyzed at wavelengths over 400 nm.[15] We therefore synthesized a DEACM-containing linker in ten steps (Scheme 2), starting with the oxidation of commercially available 7-diethylamino-4-methylcoumarin (**6**). Allylation of the aldehyde **7** provided the secondary alcohol **8**, which was then protected with a *tert*-butyldimethylsilyl (TBDMS) group and subjected to hydroboration and oxidation to afford the primary alcohol **9**. Activation with CDI followed by treatment with ethylenediamine and 2-chloroacetyl chloride yielded the intermediate **10**. The final DEACM linker **11** was then obtained after deprotection of the alcohol and coupling with *N*,*N*′-disuccinimidyl carbonate (DSC).

Since recent studies have shown that functionalization with malononitrile further red-shifts the DEACM absorption maximum,[16] we also synthesized the corresponding linker containing a diethylaminocoumarylidenemalononitrilemethyl (DEACM-MN) group in eight steps (Scheme 3). Aldehyde **7**

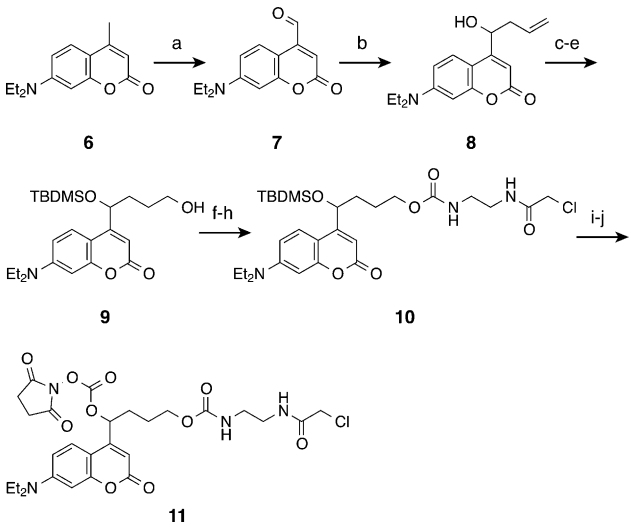

Scheme 2. DEACM linker synthesis. a) SeO_2, dioxane, 42%; allyltributylstannane, $ZnCl_2$, CH_3CN/H_2O, 83%; c) TBDMSCl, imidazole, DMF, 97%; d) $BH_3{\cdot}Me_2S$, THF; e) NaOH, H_2O_2, 49% over 2 steps; f) CDI, CH_2Cl_2; g) ethylenediamine, CH_2Cl_2; h) 2-chloroacetyl chloride, DIPEA, CH_2Cl_2, 65% over 3 steps; i) TBAF, THF, 44%; j) DSC, DMAP, CH_2Cl_2, 82%. TBAF = tetrabutylammonium fluoride, DMAP = 4-dimethylaminopyridine.

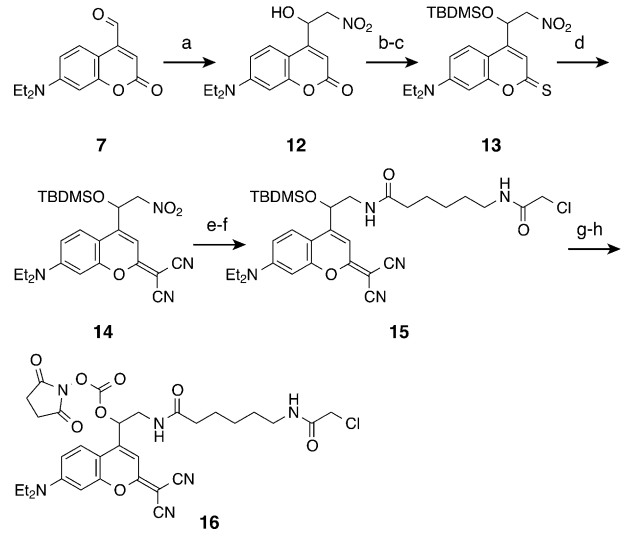

Scheme 3. DEACM-MN linker synthesis. a) CH_3NO_2, TMEDA, THF, 69%; b) TBDMSCl, imidazole, DMF, 84%; c) Lawesson's reagent, $PhCH_3$, 79%; d) malononitrile, $AgNO_3$, Et_3N, CH_3CN, 89%; e) Zn, HOAc, 70%; f) 6-(2-chloroacetamide)hexanoic acid, HATU, DIPEA, THF, 44%; g) TBAF, THF; h) DSC, DIPEA, THF, 32% over 2 steps. HATU = *N*-[[dimethylamino]-1*H*-1,2,3-triazole[4,5-*b*]-pyridin-1-ylmethylene]-*N*-methymethanamium hexafluorophosphate.

was treated with nitromethane in the presence of *N*,*N*,*N*′,*N*′-tetramethylethylenediamine (TMEDA) to afford the nitroalcohol **12**. The TBDMS-protected alcohol was converted into the corresponding thiocoumarin **13** with Lawesson's reagent, and the dicyanocoumarin **14** was obtained by silver(I)-promoted condensation with malononitrile. The nitro group was subsequently reduced with zinc and acetic acid, and the resulting amine was coupled to 6-(2-chloroace-

tamido)hexanoic acid to yield the intermediate **15**. Deprotection of the alcohol and coupling with DSC then provided the final DEACM-MN linker **16**.

We used the NB, DEACM, and DEACM-MN bifunctional linkers to prepare cMOs, by using procedures analogous to those we previously developed for DMNB-caged reagents (Scheme 4).[7] Each tether functionalized with *N*-hydroxysuccinimide ester and chloroacetamide was coupled to a *ntla*-targeting MO (5′-GACTTGAGGCAGACATATTTCCGAT-3′; anti-start codon underlined) modified with a 5′-amine and 3′-disulfide. The corresponding MO-linker amides were treated with immobilized triscarboxyethylphosphine (TCEP) to reduce the terminal disulfides, and the resulting thiols reacted spontaneously with the linker chloroacetamides to form the desired macrocycles. Any remaining linear MOs were removed from the reaction mixtures using iodoacetyl-functionalized resin, and the cyclic cMOs were purified by size-exclusion chromatography.

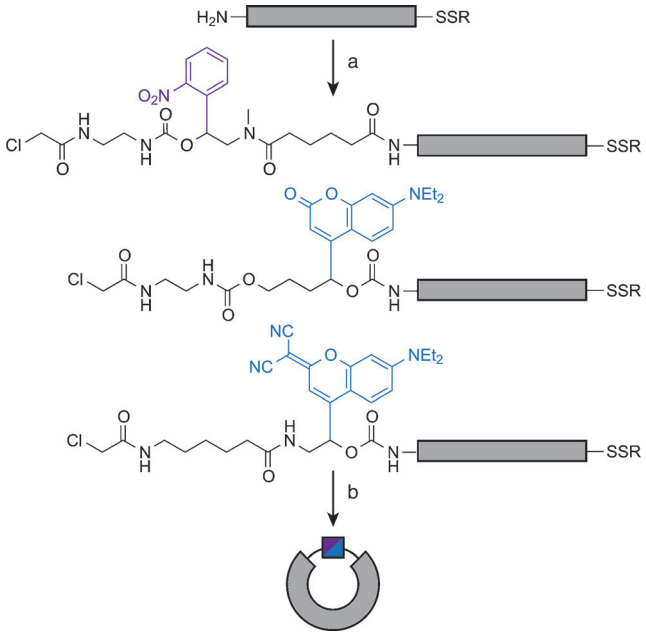

Scheme 4. Synthesis of spectrally differentiated cyclic cMOs. a) Linker **5**, **11**, or **16**, 0.1 M $Na_2B_4O_7$, pH 8.5, DMSO; b) immobilized TCEP, 0.1 M Tris·HCl, pH 8.4, 35–81% over 2 steps. Tris = tris(hydroxymethyl)aminomethane.

With these spectrally distinct cMOs in hand, we evaluated their activities in vivo. Ntla is a T-box transcription factor required for the differentiation of axial mesoderm into notochord cells (Figure 2a), and *ntla* mutants/morphants exhibit re-specification of notochord progenitors into medial floor plate cells, loss of posterior mesoderm, and mispatterned somites.[17,18] We microinjected the DMNB, NB, DEACM, and DEACM-MN cyclic *ntla* cMOs individually into zebrafish zygotes (115 fmol/embryo for all reagents except for the DEACM-MN cMO; see below) and either briefly illuminated the embryos at 3.5 h post fertilization (hpf) with 365, 405, or 470 nm light or maintained them in the dark. The zebrafish were then scored at 24 hpf for *ntla* loss-of-function phenotypes as previously described (Figure 2b).[3,7] As expected, the DMNB and NB cyclic *ntla* cMOs were efficiently uncaged by 365 nm light, thereby inducing strong *ntla*-morphant phenotypes in 89% and 86% of the embryos injected with these respective reagents (Figure 2c). The DMNB cMO was more sensitive to 405 nm light; 36% of the embryos in this cohort had partial mesodermal defects, in comparison to only 14% of the NB cMO-injected zebrafish irradiated at 405 nm. DMNB and NB cMO activation was even less efficient with 470 nm light, with 86% and 91% of the embryos developing normally under these respective conditions.

In contrast to these observations, the DEACM and DEACM-MN cyclic *ntla* cMOs were highly responsive to irradiation at 405 and 470 nm (Figure 2c). For example, 95% of the embryos injected with either reagent had morphological phenotypes consistent with a complete loss of *ntla* function upon illumination at 470 nm. The DEACM and DEACM-MN cMOs, however, were only partially activated by 365 nm light, and resulted in a range of mesodermal deficits. The DEACM-MN cMO exhibited more dark activity relative to that of its DEACM counterpart, perhaps because

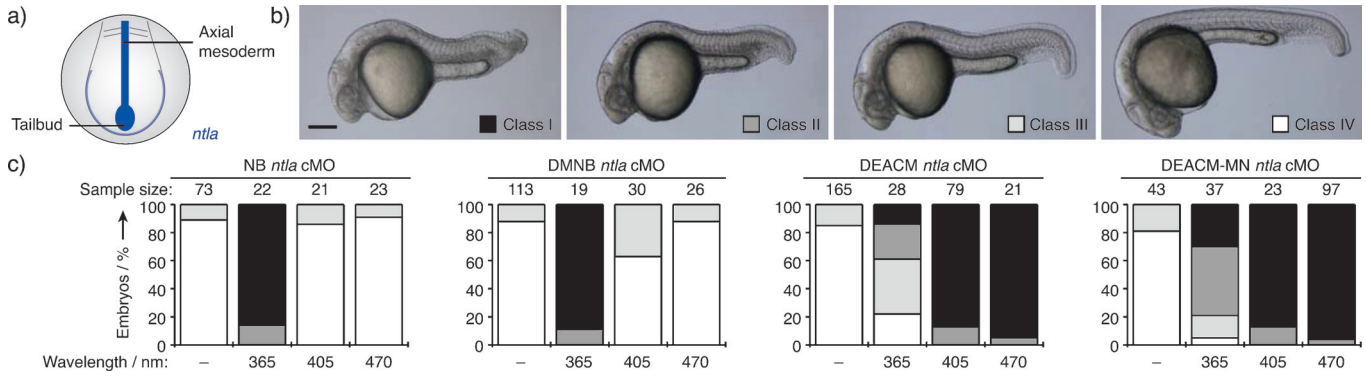

Figure 2. Comparison of NB, DMNB, DEACM, and DEACM-MN *ntla* cMOs activities in response to different irradiation wavelengths. a) Schematic representation of *ntla*-expressing cells in a 2-somite-stage zebrafish (dorsal posterior view). b) Classification of *ntla* loss-of-function phenotypes (I = most severe, IV = wild-type). 24 hpf embryos are shown (lateral view, anterior left). Scale bar: 200 μm. c) Phenotypic distributions for embryos injected with the indicated reagents and either cultured in the dark or globally irradiated with 365, 405, or 470 nm light at 3.5 hpf. No toxicity was observed with any of the cMOs or irradiation conditions.

of reduced in vivo stability. A lower embryonic dose of the malononitrile-containing reagent (87 fmol) was therefore required to minimize basal gene silencing.

Taken together, our results suggest that NB and DEACM cyclic cMOs could be used in combination to sequentially silence genes. To investigate this possibility, we focused on two additional regulators of zebrafish mesoderm development, the T-box transcription factor Spadetail (Spt/Tbx16) and the homeobox-containing repressor Floating head (Flh). Spt controls the differentiation of non-axial mesoderm, and *spt* null zebrafish lack trunk somites.[19,20] Muscle precursors in these mutants are mislocalized to the tailbud, thereby leading to the hallmark "spade tail" morphology. Spt function is largely restricted to the adaxial and paraxial mesoderm during gastrulation and somitogenesis, and its transcription within axial tissues is inhibited by Flh (Figure 3a).[21,22] Accordingly, *flh* mutants inappropriately express *spt* within the midline, which leads to the respecification of notochord progenitors into muscle.[23] The hierarchical relationship between Spt and Flh provides a convenient system for interrogating genetic interactions: *spt* mutants have reduced myogenesis, *flh* mutants exhibit ectopic axial muscle, and *spt*/*flh* double mutants phenocopy *spt* loss-of-function defects.[21]

We first recapitulated these phenotypes using conventional MOs targeting each transcription factor (*spt* MO: 5′-CTCTGATAGCCTGCATTATTTAGCC-3′; *flh* MO: 5′-GGGAATCTGCATGGCGTCT GTTTAG-3′). In comparison to wild-type zebrafish, *spt* morphants (50 fmol/embryo) were deficient in adaxial and paraxial muscle by 12 hpf, as determined by diminished expression of *myogenic differentiation 1* (*myod1*; Figure 3b,c).[24] Zebrafish injected with the *flh* MO (100 fmol/embryo) exhibited axial *myod1*-positive cells, and *spt*/*flh* double morphants had *myod1* expression patterns similar to that of embryos injected with the *spt* MO alone. We next pursued the combinatorial control of *spt* and *flh* function using spectrally differentiated cMOs. We synthesized a NB cyclic *spt* cMO and a DEACM cyclic *flh* cMO as described above, and injected the reagents into zebrafish zygotes (50 and 100 fmol/embryo, respectively), either alone or in combination. The resulting embryos were then either briefly irradiated with 365, 405, or 470 nm light at 3.5 hpf or cultured in the dark throughout their development, and we stained the embryos for *myod1* transcripts at 12 hpf. Zebrafish injected with the NB *spt* cMO alone had dramatically reduced adaxial and paraxial myogenesis upon illumination at 365 nm (100% penetrance) but minimal defects upon exposure to 405 or 470 nm light (19% and 11%, respectively; Figure 3d). Conversely, about 90% of embryos injected with the DEACM *flh* cMO had ectopic axial muscle after irradiation at 405 or 470 nm, with 365 nm light resulting in a less penetrant phenotype. To confirm that these spectral differences can be exploited to achieve sequential gene knockdowns, we co-injected the NB *spt* and DEACM *flh* cMOs into zebrafish zygotes and first irradiated the embryos at 3.5 hpf with 405 nm or 470 nm light. A subset of the animals was then exposed to 365 nm light, and the resulting *myod1* expression was scored at 12 hpf (Figure 3d). Both 405 and 470 nm irradiation selectively activated the DEACM *flh* cMO, as shown by axial *myod1* expression (75% and 83%, respectively). As expected, subsequent irradiation at 365 nm restored the *spt* loss-of-function phenotype (100% and 93%, respectively). Thus, the NB and DEACM cMOs enabled wavelength-selective control of *spt* and *flh* function in zebrafish embryos.

To conclude our studies, we utilized these spectrally differentiated cMOs to examine the timing by which ectopic *spt* function induces axial muscle development in *flh*-deficient embryos. We co-injected the NB *spt* and DEACM *flh* cMOs into zebrafish zygotes and irradiated the embryos at 3.5 hpf with 405 nm or 470 nm light to inhibit *flh* function as before. We then activated the *spt* cMO with 365 nm light at time points ranging from 5 to 7 hpf. Light-induced *spt* silencing at

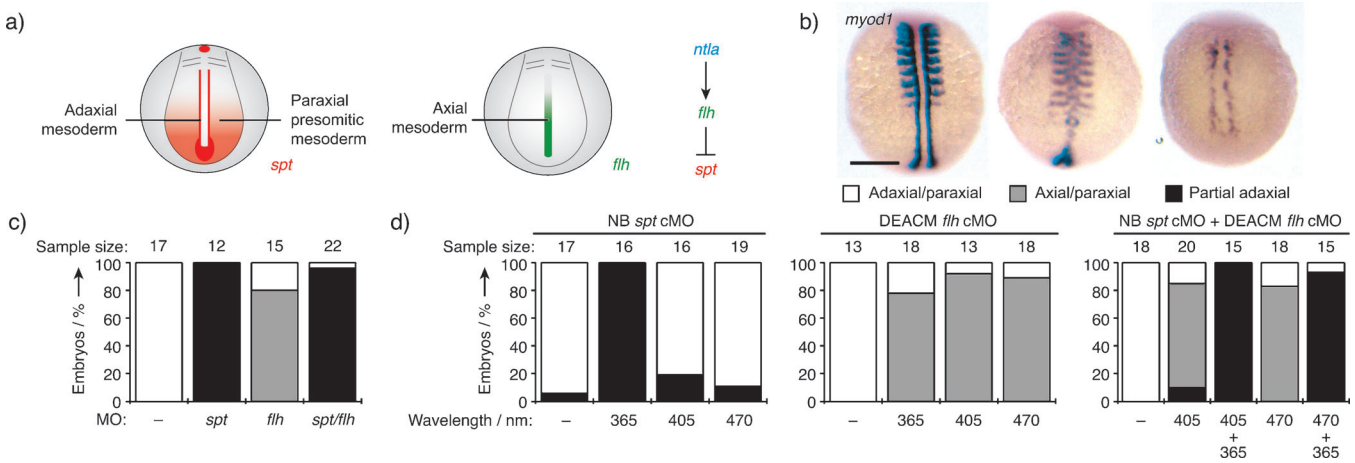

Figure 3. Combinatorial regulation of *spt* and *flh* activity using wavelength-selective cMOs. a) Schematic representation of *spt*- and *flh*-expressing cells in a 2-somite-stage zebrafish embryo (dorsal posterior view). Genetic interactions between *ntla*, *flh*, and *spt* are also shown. b) Classification of *myod1* expression patterns associated with wild-type (adaxial/paraxial), *flh* null (axial/paraxial), and *spt* null (partial adaxial) phenotypes. 12 hpf embryos are shown (dorsal view, anterior top). Scale bar: 200 μm. c) Distribution of *myod1* expression patterns in embryos injected with the indicated MOs and either cultured in the dark or globally irradiated with 365, 405, or 470 nm light at 3.5 hpf. Phenotypes were scored at 12 hpf. d) Corresponding phenotypic distributions for embryos subjected to the indicated cMOs and irradiation conditions. No toxicity was observed with any of these treatments.

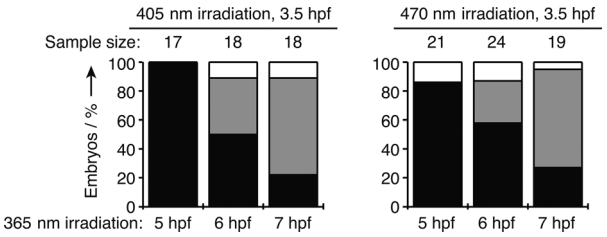

Figure 4. Sequential silencing of *flh* and *spt* using spectrally differentiated cMOs. Distribution of *myod1* expression patterns for embryos injected with NB *spt* and DEACM *flh* cMOs and subjected to dual-wavelength irradiation at different time points. Phenotypes were scored as described in Figure 3.

5 hpf resulted in nearly complete loss of adaxial and paraxial *myod1* transcription (100% and 86% penetrance for the 405 and 470 nm *flh* cMO photoactivation procedures, respectively; Figure 4). In contrast, *spt* cMO photolysis at 7 hpf predominantly yielded embryos with *flh*-morphant phenotypes (67% for both *flh* cMO uncaging procedures). Our time-course studies therefore indicate that Spt acts during gastrulation (6–9 hpf) in *flh* mutants to redirect notochord precursors toward muscle cell fates. This action precedes axial *myod1* expression in *flh* mutants, which is evident by the 3- to 5-somite stage (10–11 hpf).[23]

In summary, we have achieved the first sequential inactivation of organismal gene function using reverse-genetic chemical probes. Our studies demonstrate that NB- and DEACM-based cyclic cMOs can be differentially activated by 365 and 405/470 nm light, thereby expanding the scope of caged antisense technologies. Such synthetic tools complement TALEN (transcription activator-like effector nucleases) and CRISPR (clustered regularly interspaced short palindromic repeats)/Cas genome-editing technologies, which have been successfully employed in zebrafish.[25,26] Cyclic cMOs can be synthesized and applied within days, thus allowing rapid loss-of-function studies with nearly complete phenotypic penetrance and a high degree of spatial, temporal, and dosage control. In comparison, genetic approaches can require multiple animal generations for full implementation, have more limited conditionality, and are subject to Mendelian phenotypic frequencies.

We anticipate that these optochemical tools will be valuable probes of the genetic interactions that dynamically regulate tissue formation and function. The commercial availability of 5′-amine- and 3′-disulfide-functionalized MOs and the ease with which they can be cyclized should make this chemical approach widely available to the scientific community. Our MO caging strategy is also compatible with a variety of linkers, thereby facilitating the implementation of other chromophores. As new caging groups with divergent spectral properties continue to be developed,[27] it is likely that future cMO technologies will eventually enable the orthogonal photoregulation of three or more genes.

Received: May 16, 2014
Published online: August 1, 2014

Keywords: antisense agents · cage compounds · developmental biology · gene expression · oligonucleotides

[1] C. Brieke, F. Rohrbach, A. Gottschalk, G. Mayer, A. Heckel, *Angew. Chem.* **2012**, *124*, 8572 – 8604; *Angew. Chem. Int. Ed.* **2012**, *51*, 8446 – 8476.
[2] I. A. Shestopalov, S. Sinha, J. K. Chen, *Nat. Chem. Biol.* **2007**, *3*, 650 – 651.
[3] X. Ouyang, I. A. Shestopalov, S. Sinha, G. Zheng, C. L. Pitt, W. H. Li, A. J. Olson, J. K. Chen, *J. Am. Chem. Soc.* **2009**, *131*, 13255 – 13269.
[4] A. J. Tomasini, A. D. Schuler, J. A. Zebala, A. N. Mayer, *Genesis* **2009**, *47*, 736 – 743.
[5] A. Deiters, R. A. Garner, H. Lusic, J. M. Govan, M. Dush, N. M. Nascone-Yoder, J. A. Yoder, *J. Am. Chem. Soc.* **2010**, *132*, 15644 – 15650.
[6] A. Tallafuss, D. Gibson, P. Morcos, Y. Li, S. Seredick, J. Eisen, P. Washbourne, *Development* **2012**, *139*, 1691 – 1699.
[7] S. Yamazoe, I. A. Shestopalov, E. Provost, S. D. Leach, J. K. Chen, *Angew. Chem.* **2012**, *124*, 7014 – 7017; *Angew. Chem. Int. Ed.* **2012**, *51*, 6908 – 6911.
[8] Y. Wang, L. Wu, P. Wang, C. Lv, Z. Yang, X. Tang, *Nucleic Acids Res.* **2012**, *40*, 11155 – 11162.
[9] I. A. Shestopalov, C. L. Pitt, J. K. Chen, *Nat. Chem. Biol.* **2012**, *8*, 270 – 276.
[10] J. C. Moore, S. Sheppard-Tindell, I. A. Shestopalov, S. Yamazoe, J. K. Chen, N. D. Lawson, *Dev. Biol.* **2013**, *384*, 128 – 140.
[11] N. Kotzur, B. Briand, M. Beyermann, V. Hagen, *J. Am. Chem. Soc.* **2009**, *131*, 16927 – 16931.
[12] M. A. Priestman, L. Sun, D. S. Lawrence, *ACS Chem. Biol.* **2011**, *6*, 377 – 384.
[13] S. Kantevari, M. Matsuzaki, Y. Kanemoto, H. Kasai, G. C. Ellis-Davies, *Nat. Methods* **2010**, *7*, 123 – 125.
[14] B. N. Goguen, A. Aemissegger, B. Imperiali, *J. Am. Chem. Soc.* **2011**, *133*, 11038 – 11041.
[15] P. Bourbon, Q. Peng, G. Ferraudi, C. Stauffacher, O. Wiest, P. Helquist, *J. Org. Chem.* **2012**, *77*, 2756 – 2762.
[16] L. Fournier, I. Aujard, T. Le Saux, S. Maurin, S. Beaupierre, J. B. Baudin, L. Jullien, *Chem. Eur. J.* **2013**, *19*, 17494 – 17507.
[17] M. E. Halpern, R. K. Ho, C. Walker, C. B. Kimmel, *Cell* **1993**, *75*, 99 – 111.
[18] S. Schulte-Merker, F. J. van Eeden, M. E. Halpern, C. B. Kimmel, C. Nusslein-Volhard, *Development* **1994**, *120*, 1009 – 1015.
[19] R. K. Ho, D. A. Kane, *Nature* **1990**, *348*, 728 – 730.
[20] K. J. Griffin, S. L. Amacher, C. B. Kimmel, D. Kimelman, *Development* **1998**, *125*, 3379 – 3388.
[21] S. L. Amacher, C. B. Kimmel, *Development* **1998**, *125*, 1397 – 1406.
[22] A. Yamamoto, S. L. Amacher, S. H. Kim, D. Geissert, C. B. Kimmel, E. M. De Robertis, *Development* **1998**, *125*, 3389 – 3397.
[23] M. E. Halpern, C. Thisse, R. K. Ho, B. Thisse, B. Riggleman, B. Trevarrow, E. S. Weinberg, J. H. Postlethwait, C. B. Kimmel, *Development* **1995**, *121*, 4257 – 4264.
[24] E. S. Weinberg, M. L. Allende, C. S. Kelly, A. Abdelhamid, T. Murakami, P. Andermann, O. G. Doerre, D. J. Grunwald, B. Riggleman, *Development* **1996**, *122*, 271 – 280.
[25] L. Cade, D. Reyon, W. Y. Hwang, S. Q. Tsai, S. Patel, C. Khayter, J. K. Joung, J. D. Sander, R. T. Peterson, J. R. Yeh, *Nucleic Acids Res.* **2012**, *40*, 8001 – 8010.
[26] W. Y. Hwang, Y. Fu, D. Reyon, M. L. Maeder, P. Kaini, J. D. Sander, J. K. Joung, R. T. Peterson, J. R. Yeh, *PLoS One* **2013**, *8*, e68708.
[27] J. P. Olson, M. R. Banghart, B. L. Sabatini, G. C. Ellis-Davies, *J. Am. Chem. Soc.* **2013**, *135*, 15948 – 15954.

